Available online at www.sciencedirect.com
ScienceDirect
Journal of Power Sources 158 (2006) 1333–1343
JOURNAL OF POWER SOURCES
www.elsevier.com/locate/jpowsour

Dynamic centrifugal compressor model for system simulation

Wei Jiang *, Jamil Khan, Roger A. Dougal

Department of Mechanical Engineering, University of South Carolina, Columbia, SC 29208, United States

Received 9 June 2005; received in revised form 25 October 2005; accepted 26 October 2005
Available online 27 December 2005

Abstract

A dynamic model of a centrifugal compressor capable of system simulation in the virtual test bed (VTB) computational environment is presented. The model is based on first principles, i.e. the dynamic performance including the losses is determined from the compressor geometry and not from the experimentally determined characteristic performance curves. In this study, the compressor losses, such as incidence and friction losses, etc., are mathematically modeled for developing compressor characteristics. For easy implementation in the VTB platform, the non-linear governing equations are discretized in resistive companion (RC) form. The developed simulation model can be applied to virtually any centrifugal compressor. By interfacing with a composite system, such as a Brayton cycle gas turbine, or a fuel cell, the compressor dynamic performance can be evaluated. The surge line for the compressor can also be determined from the simulation results. Furthermore, the model presented here provides a valuable tool for evaluating the system performance as a function of various operating parameters.

Keywords: Centrifugal compressor; Dynamic model; Resistive companion method; Virtual test bed; Simulation; Incidence loss

1. Introduction

Analytical performance prediction method plays an important role in designing a centrifugal compressor by way of predicting the overall dimensions and performance curve of the stage. First of all, the analytical method can be used to perform parametric studies to demonstrate the influence of changes in geometry on the performance under both design and off-design conditions. Therefore, the availability of reliable analytic tool saves expensive experimental development. In addition, analytic models for predicting the overall performance of the compressor can be effectively used in predicting the overall performance of a combination system where the compressor is a component of such a system.

In order to derive the analytical tools, the losses occurring throughout the stage must be specified. The origin and effects of loss mechanism were discussed in details in references [4–6]. These papers presented prediction methods based on modeling various losses throughout the stage. According to references [1,2,7], the losses in the centrifugal compressor are classified into incidence loss, friction loss, clearance loss, backward loss and volute loss. Reference [3] presents comparative study of the existing modeling techniques and their limitations for predicting incidence loss. There are two widely used models: one is the constant pressure incidence model and the other is the NASA shock loss theory as described in references [2,3]. In the current study, the NASA shock loss theory is used. It can be mentioned here that very little difference exists between the two models for centrifugal compressor as expounded in reference [1]. As to the friction loss, references [2,3] apply the energy and momentum equations to pipe flow with surface frictions to get the loss coefficient related with Reynolds number. For this study, we used the approach of references [2,3] to predict the friction loss.

The virtual test bed (VTB) provides an effective computational environment to simulate the dynamic performance of the centrifugal compressor [12]. The non-linear model equations based on energy transfer are discretized in resistive companion (RC) form for effective implementation in the VTB platform. After the compressor model is developed and validated; a dynamic simulations of a fuel–cell system assembled in the VTB environment are carried out to analyze the compressor performance along with the system performance. Details of VTB is given in reference [11,13].

The remainder of this paper is organized as follows. The mathematical identify equations for the centrifugal compressor

* Corresponding author. Tel.: +1 803 777 0838; fax: +1 803 777 0106.
E-mail address: jiangw@engr.sc.edu (W. Jiang).

0378-7753/$ – see front matter © 2005 Elsevier B.V. All rights reserved.
doi:10.1016/j.jpowsour.2005.10.093

Nomenclature

a	hydraulic perimeter (m)
A_1	absolute inlet velocity (m s^{-1})
C_p	specific heat (kg kJ^{-1} K^{-1})
C_{r1}	inlet radial velocity of fluid (m s^{-1})
C_{r2}	outlet radial velocity of fluid (m s^{-1})
C_1	absolute inlet velocity (m s^{-1})
C_{2i}	the loss of outlet tangential velocity of fluid (m s^{-1})
$C_{\theta 1}$	inlet tangential velocity of fluid (m s^{-1})
$C_{\theta 2}$	outlet tangential velocity of fluid (m s^{-1})
D	mean hydraulic channel diameter (m)
D_{h1}	hub casing diameter (m)
D_{t1}	inducer tip diameter (m)
D_1	inlet average diameter (m)
D_2	outlet average diameter (m)
f	friction factor
$\dot{m}$	mass flow rate (kg s^{-1})
J	spool moment of the inertia (kg m^2)
l	mean channel length (m)
p_0	inlet pressure of compressor (Pa)
p_2	outlet pressure of compressor (Pa)
r_1	inlet average radius (m)
r_2	outlet average radius (m)
Re	mean Reynolds number
T_0	inlet temperature of compressor (K)
T_2	outlet temperature of compressor (K)
U	blade tangential velocity (m s^{-1})
U_1	the inlet tangential velocity of the impeller (m s^{-1})
U_2	the outlet tangential velocity of the impeller (m s^{-1})
W_c	power delivered to the fluid (J)
W_1	ideal inlet relative velocity (m s^{-1})
W_{1b}	actual inlet relative velocity (m s^{-1})
$W_{\theta 1}$	the loss of relative inlet tangential velocity (m s^{-1})
α_2	fluid inlet angle (°)
α_{2b}	blade outlet angle (°)
β_1	fluid inlet angle (°)
β_{1b}	blade inlet angle (°)
Δh_{bf}	backflow loss (J kg^{-1})
Δh_{cl}	clearance loss (J kg^{-1})
Δh_{df}	friction loss for diffuser (J kg^{-1})
Δh_f	friction loss (J kg^{-1})
Δh_i	incidence loss (J kg^{-1})
Δh_{id}	incidence loss for diffuser (J kg^{-1})
Δh_{ideal}	ideal specific enthalpy delivered to the fluid (J kg^{-1})
Δh_{if}	friction loss for inducer (J kg^{-1})
Δh_{ii}	incidence loss for inducer (J kg^{-1})
Δh_v	volute loss (J kg^{-1})
$\Delta \eta_{bf}$	efficiency loss increases with backflow
$\Delta \eta_{cl}$	efficiency loss increases with clearance
$\Delta \eta_v$	efficiency loss increases with volute
γ	specific heat ratio
η_i	efficiency
ρ_{01}	constant stagnation inlet density (kg m^{-3})
σ	slip factor
τ_c	compressor torque (N m)
τ_t	drive torque (N m)
ω	rotational speed (rpm)

are presented in Section 2. The RC model formulation is derived in Section 3. Section 4 gives the simulation results of compressor. In Section 5, discussion of the performance and analysis of the compressor in the overall fuel–cell system are presented. Conclusions are made in Section 6.

2. Identify equations

Energy transfer is mainly considered in developing compressor characteristic. The fluid enters the compressor rotor at one radius with one velocity and leaves at another radius with another velocity. The change in momentum of the fluid is derived from the work done by the rotating rotor, which is driven by an externally applied torque. The compressor characteristic equation can be described as follows:

$$\dot{\omega} = \frac{1}{J} \cdot (\tau_t - \tau_c) \tag{1}$$

$$\omega \cdot \tau_c = W_c = \dot{m} \cdot \Delta h_{ideal} \tag{2}$$

$$p_2 = \left(1 + \frac{\eta_i(\dot{m}, U) \cdot \Delta h_{ideal}}{T_0 \cdot C_p}\right)^{\gamma/(\gamma-1)} \cdot p_0 \tag{3}$$

$$\Delta h_{ideal} = \frac{\dot{W}_c}{\dot{m}} = \sigma \cdot U_2^2 \tag{4}$$

Eq. (1) presents momentum torque equation. The difference between external drive torque τ_t and compressor torque τ_c used to change the fluid momentum is expended to cause the rotor to rotate.

Eq. (2) comes from the Euler's pump equation, where $\dot{m}$ is the mass flow rate of the compressor. The specific enthalpy Δh_{ideal} delivered to the fluid should be equal to the power delivered to the fluid W_c.

Eq. (3) is derived from isentropic compression relations between pressure and temperature. Various kinds of losses are considered in determining the efficiency η_i ($\dot{m}$, U, which is a function of the mass flow rate and rotational speed).

Eq. (4) further specifies the specific enthalpy Δh_{ideal}, where we assume that there are no stationary pre-whirl vanes and air approaching the impeller does not have a tangential component of velocity. σ is called the slip factor, the ratio between outlet tangential velocity of the fluid $C_{\theta 2}$ and the outlet tangential velocity of the impeller U_2. For the details of the derivation of Eq. (4), please refer to Appendix A.

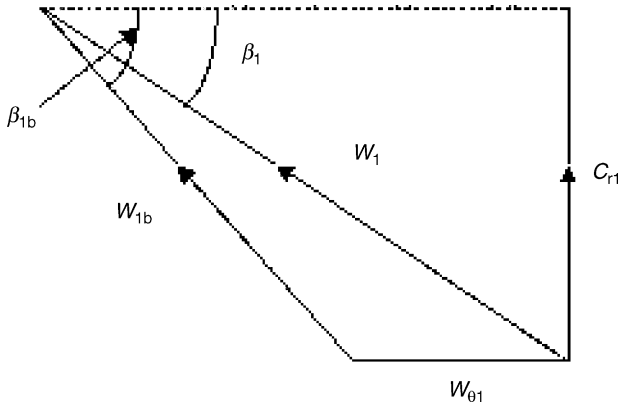

Fig. 1. Incidence loss for fluid entering inducer.

2.1. Loss modeling

2.1.1. Incidence losses

Incidence losses come from the off-design velocity triangles at the impeller eye (inducer) causing flow separation and are therefore at the design point this loss is zero.When the fluid is entering the impeller eye at a relative velocity of W_1 and with an inlet angle β_1, as shown in Fig. 1, it is assumed that the fluid instantaneously changes its direction to comply with the blade inlet angle β_{1b}. As a result, the relative velocity of the fluid is changed from W_1 to W_{1b}. According to references [2,3], NASA theory it is assumed that the kinetic energy associated with tangential component $W_{\theta 1}$ is destroyed as the fluid adapts to the blade direction. Thus, the energy loss due to incidence is given by

$$\Delta h_{ii} = \frac{W_{\theta 1}^2}{2} \tag{5}$$

From Fig. 1, it can be shown that

$$\cos\beta_1 = \frac{U_1 - C_{\theta 1}}{W_1} \quad \text{and} \quad \sin\beta_1 = \frac{C_{r1}}{W_1} \tag{6}$$

where $C_{\theta 1}$ and C_{r1} are the inlet tangential velocity and inlet radial velocity of fluid, respectively, and

$$W_{\theta 1} = \frac{\sin(\beta_{1b} - \beta_1)}{\sin\beta_{1b}} W_1 = (\cos\beta_1 - \cot\beta_{1b}\ \sin\beta_1) \cdot W_1 \tag{7}$$

From Eqs. (6) and (7)

$$W_{\theta 1} = U_1 - C_{\theta 1} - \cot\beta_{1b}\, c_{r1} \tag{8}$$

So the incidence loss can be written as

$$\Delta h_{ii} = \frac{1}{2}(U_1 - C_{\theta 1} - \cot\beta_{1b}\, c_{r1})^2 = \frac{1}{2}\left(U_1 - \frac{\cot\beta_{1b}\, \dot{m}}{\rho_{01} A_1}\right)^2 \tag{9}$$

Similar to the flow situation in the impeller, when the fluid enters the vane diffuser at a velocity of C_2 and with an inlet angle α_2, as shown in Fig. 2, it is assumed that the fluid instantaneously changes its direction to comply with the diffuser inlet angle α_{2b}. As a result, the velocity of the fluid is changed from C_2 to C_{2b}. According to reference [1,10], the kinetic energy associated with the tangential component C_{2i} of the velocity is lost. So the incidence loss can be expressed as

$$\Delta h_{id} = \frac{C_{2i}^2}{2} \tag{10}$$

From Fig. 2, we can obtain

$$\Delta h_{id} = \frac{1}{2}(\sigma U_2 - \cot\alpha_{2b}\, C_{r2})^2 \tag{11}$$

where C_{r2} is the outlet radial velocity of the fluid and $C_{\theta 2}$ is the outlet tangential velocity of fluid.

For simplicity, we further assume that $C_{r1} = C_{r2}$.

$$U_1 = C_{r1}\ \cot\beta_{1b} \Rightarrow C_{r2} = U_1\ \tan\beta_{1b} \tag{12}$$

From Fig. 2, it follows that

$$\tan\alpha_{2b} = \frac{C_{r2}}{C_{\theta 2}} = \frac{U_1\ \tan\beta_{1b}}{\sigma U_2} \tag{13}$$

So

$$\alpha_{2b} = a\ \tan\left(\frac{D_1\ \tan\beta_{1b}}{\sigma D_2}\right) \tag{14}$$

and according to the above equations the diffuser incidence loss can be written as

$$\Delta h_{id} = \frac{1}{2}\left(\frac{\sigma D_2 U_1}{D_1} - \frac{m \cdot \cot\alpha_{2b}}{\rho_{10} A_1}\right) \tag{15}$$

2.1.2. Friction losses

According to reference [2], the friction loss in the impeller can be defined as

$$\Delta h_f = 4f\frac{l}{D}\frac{W_{1b}^2}{2} \tag{16}$$

where f is the friction factor for appropriate mean Reynolds number, l the mean channel length and D is the mean hydraulic channel diameter, which is defined as

$$f = 0.3164(Re)^{-0.25} \tag{17}$$

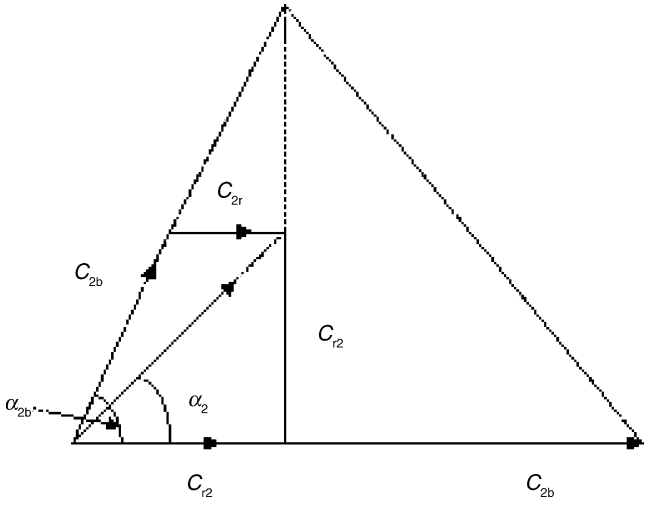

Fig. 2. Incidence losses of fluid entering diffuser.

The mean hydraulic channel D is defined as

$$D = \frac{4A}{a} \tag{18}$$

From Fig. 2, it is seen that

$$\frac{W_{1b}}{\sin\beta_1} = \frac{W_1}{\sin\beta_{1b}} \tag{19}$$

and using $\sin\beta_1 = (C_{r1}/W_1)$, we can get

$$W_{1b} = \frac{C_1}{\sin\beta_{1b}} \tag{20}$$

Finally, we can get the friction loss at impeller

$$\Delta h_{if} = k_{fi}\dot{m}^2 = \frac{C_h l}{2D\rho_1^2 A_1^2 \sin^2\beta_{1b}}\dot{m}^2 \tag{21}$$

For diffuse the friction loss can be modeled in a similar manner as in the impeller

$$\Delta h_{df} = k_{fd}\dot{m}^2 = \frac{C_h l}{2D\rho_1^2 A_1^2 \sin^2\beta_{1b}}\dot{m}^2 \tag{22}$$

2.1.3. Other losses

According to reference [2], the clearance loss is a function of the clearance to passage width at the tip. Pampreen showed that the stage efficiency loss increases with clearance and can be expressed as $\Delta\eta_{cl} \approx 0.3(l_{c1}/b_2)$, where l_{cl} is the tip axial clearance and b_2 is the impeller tip width. For back flow loss, no theory or mathematical model exists at present to describe the backflow loss, Dean and Young suggested a backflow loss of three points of stage efficiency as typical: $\Delta\eta_{bf} = 0.03$. According to reference [1], the volute loss is assumed to lie within two to five point of efficiency: $0.02 \le \Delta\eta_v \le 0.05$. According to simulation results of this paper, under the operating conditions of a rotational speed of 35,000 rpm and in the neighborhood of the surge line, the relative magnitudes of clearance, backflow and volute losses are 13.33, 12.5 and 14.58%, respectively, of the total loss. It should be noted that the relative magnitudes of clearance, backflow and volute losses will decrease gradually as mass flow rate goes up, this is due to the fact that at higher mass flow rates the incidence loss and friction loss will increase.

2.2. Efficiency

The isentropic efficiency of the compressor is defined as

$$\eta_i(\dot{m}, U) = \frac{\Delta h_{ideal}}{\Delta h_{ideal} + \Delta h_{loss}} - \Delta\eta_{cl} - \Delta\eta_{bf} - \Delta\eta_v \tag{23}$$

where in this paper, the loss Δh_{loss} is equal to the sum of incidence losses and friction losses.

$$\Delta h_{loss} = \Delta h_{ii} + \Delta h_{di} + \Delta h_{if} + \Delta h_{df} \tag{24}$$

3. RC model formulation

The resistive-companion method [8,9] provides a way to account for natural conservation laws by defining a pair of across and through variables at each terminal. The device object interacts with the VTB network solver by providing the device conductance matrix and the history vector at each simulation time steps, so that the solution to the entire circuit can be sought by the solver based on the mathematically equivalent nodal circuit analysis. The solver requires that the relations of the terminal variables for each device be written in the following standard form:

$$I(t) = G \cdot V(t) - B(t-h) \tag{25}$$

where $I(t)$ is the through variable vector, $V(t)$ the across variable vector, G the conductance matrix, $B(t-h)$ the history vector of the device and h is the simulation time step. Notice that although the term "conductance matrix", inherited from electric network analysis, is used, the terminal variables are more generally across and through variables, not necessarily voltage and current.

In Fig. 3, it is shown that the compressor interacts with the external world through its two terminals. Node 0 is a mechanical terminal where torque τ is through variable and rotational speed ω is an across variable, through which compressor connects with outer driving machine such as a motor or a gas turbine. Node 1 is a fluid terminal where mass flow rate $\dot{m}$ is a through variable and pressure p is an across variable, by which compressed fluid is outputted.

Eq. (1), $\dot{\omega} = \frac{1}{J}\cdot(\tau_t - \tau_c)$, is discretized within one time step using trapezoidal method.

$$\tau_t(t) = \frac{2J}{h}\omega(t) + \tau_c(t) - \frac{2J}{h}\omega(t-h) - \tau_t(t-h) + \tau_c(t-h) \tag{26}$$

For the non-linear equations (2) and (3), Newton–Raphson iterations is introduced to solve these equations. By eliminating the intermediate variables τ_c, $\eta_i(\dot{m}, U)$ and Δh_{ideal}, we can obtain standard RC equations presented below:

$$\begin{pmatrix}\dot{m}(t)\\ \tau_t(t)\end{pmatrix} = \begin{pmatrix}\frac{\partial\dot{m}}{\partial p_2} & \frac{\partial\dot{m}}{\partial\omega}\\ \frac{\partial\tau_t}{\partial p_2} & \frac{\partial\tau_t}{\partial\omega}\end{pmatrix}_{t-h} \cdot \begin{pmatrix}p_2(t)\\ \omega(t)\end{pmatrix} - \begin{pmatrix}b_0(t-h)\\ b_1(t-h)\end{pmatrix} \tag{27}$$

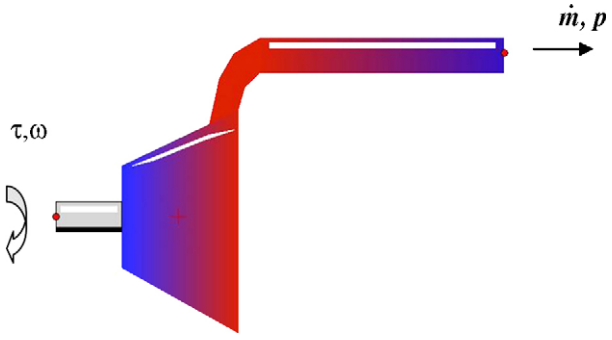

Fig. 3. Centrifugal compressor icon in VTB.

where the history for $\dot{m}$ is

$$b_0(t-h) = -\dot{m}(t-h) + \frac{\partial \dot{m}}{\partial p_2} \cdot p_2(t-h) + \frac{\partial \dot{m}}{\partial \omega} \cdot \omega(t-h) \tag{28}$$

$$b_1(t-h) = -\tau_t(t-h) + \frac{\partial \tau_t}{\partial p_2} \cdot p_2(t-h) + \frac{\partial \tau_t}{\partial \omega} \cdot \omega(t-h) \tag{29}$$

Finally, we can obtain the complete RC model equations (27)–(29) for the centrifugal compressor.

4. VTB simulation

An integrated hybrid solid oxide fuel cell energy system, assembled in the VTB environment, is shown in Fig. 4. The centrifugal compressor is driven by a motor, and the compressed air is supplied to fuel cell. The system consists of a fuel compressor, an air compressor, a fuel cell, a combustor, a gas turbine, a heat exchanger and a fuel tank. The compressed air is pre-heated by a heat exchanger prior to entering the fuel cell, where the natural gas is internally reformed. After the electrochemical reaction, electrical energy is produced which is associated with simultaneous heat generation during the process. For further extraction of energy the un-reacted high-temperature gases are channeled to the combustor for complete combustion there. The exhaust gas then expands through the gas turbine whereby mechanical power is generated. The exhaust gas discharging from the gas turbine is further used for the purpose of regeneration, by passing it through the heat exchanger where it pre-heats the compressed air going to the fuel cell stacks. The load of the compressor depends on the number of cells. The output of this fuel cell system, in the form of electrical power, is supplied to an electrical circuit load. It can be mentioned here that for the fuel–cell system the compressor had a flow rate of less than 1 kg s^{-1}, pressure ratio of less than 4, and the maximum compressor power of 332 kW and power generated by the overall system was less than 1 MW. The modeling details for the fuel cell and other components are not presented in this paper because the focus of this paper is the centrifugal compressor modeling.

The physical dimensions of some of the parameters of the centrifugal compressor used in this system are listed in Table 1.

The simulation results obtained in VTB are presented as four representative curves, as shown in Fig. 5, including the mass flow

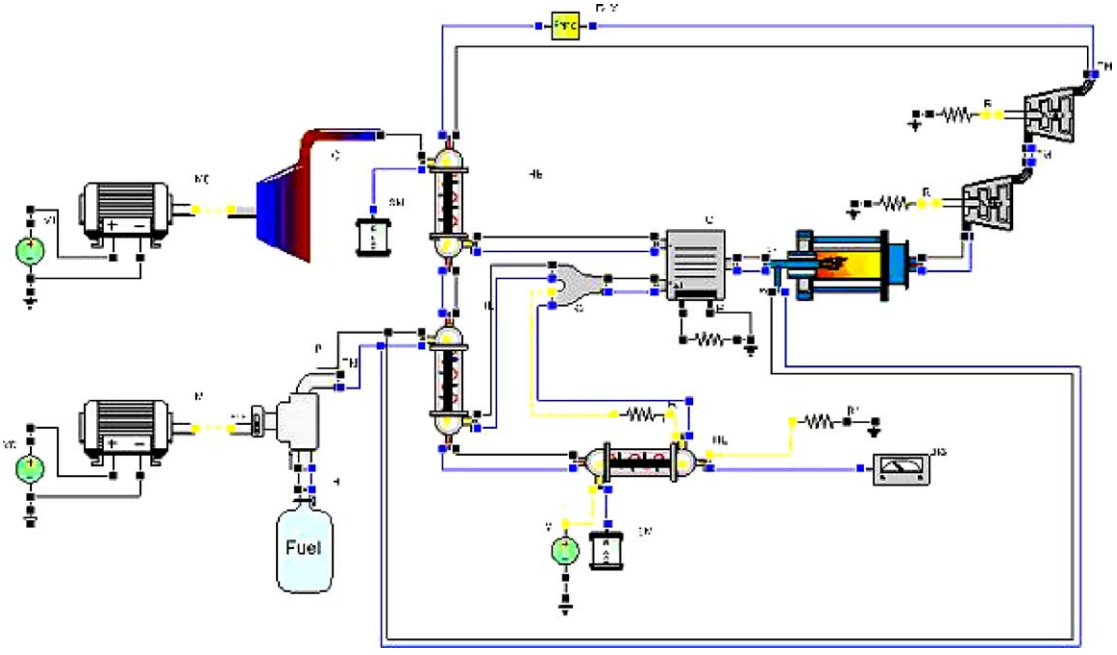

Fig. 4. Simulation system.

Table 1
Parameters for dynamic centrifugal compressor model

Parameter	Value	Parameter	Value
Slip coefficient	0.9	Outlet tip diameter (m)	0.15
Blade inlet angle (°)	45	Outlet hub diameter (m)	0.10
Diffuser inlet angle (°)	45	Mean impeller channel length (m)	0.12
Inlet tip diameter (m)	0.07	Mean diffuser channel length (m)	0.1
Inlet hub diameter (m)	0.034	Spool moment of inertia (kg m^2)	5
Pressure atmosphere (Pa)	101,000	Temperature atmosphere (K)	298
Density of the fluid (kg m^{-3})	1.205	Kinetic viscosity of the fluid (m^2 s^{-1})	0.001

Fig. 5. Dynamic simulation results obtained in VTB.

rate, output pressure, rotational speed and efficiency, each of which is displayed, respectively, as a function of time in seconds. The rotational speed and efficiency curves start from zero and reach a steady state at the end. Meanwhile, the output pressure increases from the atmospheric pressure to a steady-state value. The magnitude of mass flow rate is mainly decided by the fuel cell.

5. Discussion

5.1. Compressor characteristics

Further derivation based on the VTB simulation results leads to compressor characteristics curves with a specific set of parameters. The extensive characteristics curves studies can be performed by intentionally changing the compressor parameters as needed. The resulting analysis lays a solid foundation for the behavior prediction of the compressor.

Fig. 6a shows efficiency versus mass flow rate characteristics obtained from simulation under different rotational speeds N, ranging from 20,000 to 50,000 rpm. The observations from the figure are listed as follows:

- The optimum mass flow rate, i.e. best efficiency of the compressor changes a function of rotational speed. For example, the optimum mass flow rate is around 0.15 kg s^{-1} in the case of 20,000 rpm rotational speed and it changes to 0.3 kg s^{-1} in the case of 50,000 rpm rotational speed.
- The optimum mass flow rate increases as the rotational speed goes up.
- Under a specific rotational speed, in case that the mass flow rate is beyond the optimum value, the efficiency of the compressor begins to decrease as the mass flow rate increases. And this phenomenon gets more pronounced at lower rotational speeds.
- Thus, based on the first two observations, for a given mass flow rate in the real case, the optimum characteristics of the compressor can be achieved by adjusting the rotational speed N.
- Based on the third observation, it is apparent that operating under higher rotational speed leads to a better efficiency especially for larger mass flow rates.

Fig. 6b presents outlet pressure versus mass flow rate characteristics obtained from simulation under different rotational speeds N, ranging from 20,000 to 50,000 rpm. The observations from the figure are listed as follows:

- The outlet pressure is a function of the mass flow rate and rotational speed N. Therefore, the desired outlet pressure can be achieved by regulating either the mass flow rate or the rotational speed or both of them.
- The rotational speed imposes a much bigger effect on the outlet pressure than that of the mass flow rate. As a result, adjustment of the rotational speed works more favorably for the macro-adjustment of the outlet pressure while the regulation of the mass flow rate would be preferable for the micro-adjustment of the outlet pressure.

Fig. 6c illustrates incidence loss versus mass flow rate characteristics obtained from simulation under different rotational speeds N, ranging from 20,000 to 50,000 rpm. The observations from the figure are listed as follows:

- Incidence loss decreases at first till it reaches minimum value, i.e. the on-design working point without incidence loss. The existence of the zero incidence loss is explained by the fact that the change of the mass flow rate affects the fluid velocity; this change further influences the fluid inlet angle. When the fluid inlet angle coincides

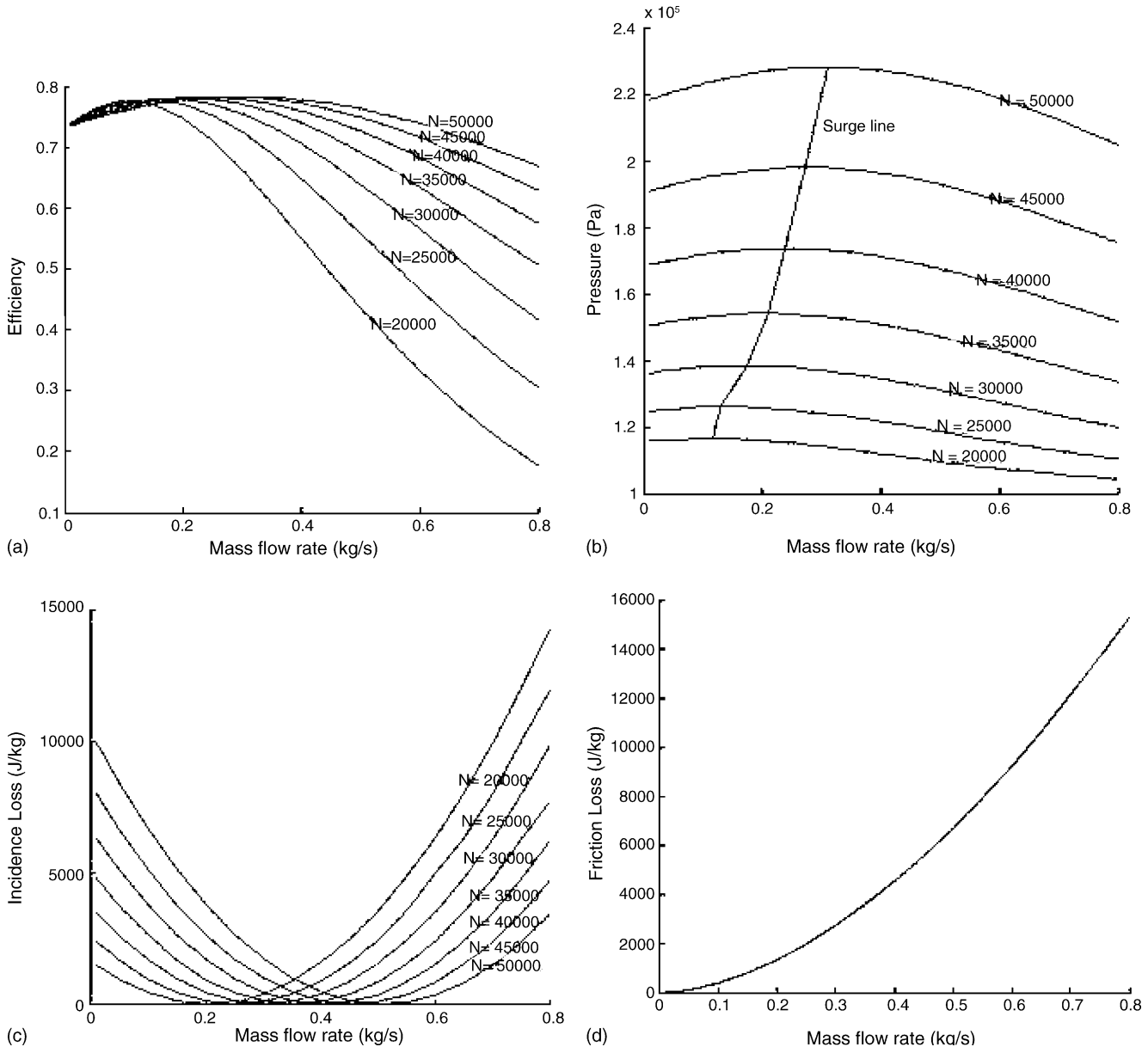

Fig. 6. (a) $\dot{m}$ vs. efficiency for various rotational speed; (b) $\dot{m}$ vs. pressure for various rotational speed; (c) $\dot{m}$ vs. incidence loss for various rotational speed; (d) $\dot{m}$ vs. friction loss for various rotational speed.

with the blade inlet angle, the incidence loss becomes zero.

- Different rotational speed leads to different zero incidence loss point. Since the fluid inlet angle is a function of both mass flow rate and rotational speed, the mass flow rate needs to be regulated accordingly as the rotational speed changes so as to maintain the coincidence of the fluid inlet angel with the blade inlet angle.

Fig. 6d depicts friction loss versus mass flow rate characteristics obtained from simulation under various rotational speeds N, ranging from 20,000 to 50,000 rpm. The overlapping of all the curves indicates that frictional loss is a function of mass flow rate only and that the change of the rotational speed has no bearing on the friction losses.

5.2. Parameters analysis

Parametric analysis plays a very important role in the design of compressors. With the analytical method applied to parametric studies, it is easy to demonstrate the influence of changes in geometry on the performance under both design and off-design conditions, thus providing the guideline for compressor optimization without expensive and time-consuming experimental efforts.

Fig. 7 demonstrates outlet pressure versus mass flow rate (a) and efficiency versus mass flow rate characteristics curve (b) with different slip factors while all the other parameters were kept unchanged. As shown in the figures, both the outlet pressure and efficiency decrease when slip factor changes from 0.9 to 0.8. This implies that,

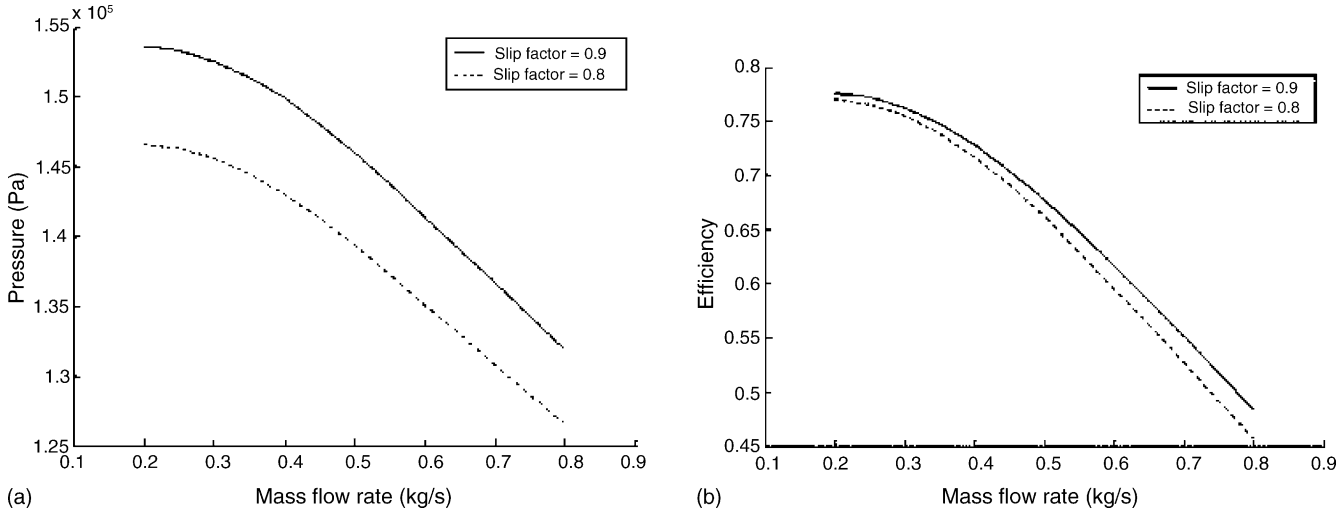

Fig. 7. (a) $\dot{m}$ vs. pressure for two different slip factors and (b) $\dot{m}$ vs. efficiency for two different slip factors.

a larger slip factor translates into better compressor efficiency.

Fig. 8 shows outlet pressure versus mass flow rate (a) and efficiency versus mass flow rate (b) characteristics curve at different inlet and outlet diameters. The exact parameters for various cases are listed in Table 2. As shown in Fig. 8a, with all the other parameters remaining unchanged, smaller diameter produces smaller outlet pressure. As observed from (b), the effect of diameter size on the efficiency is weak when mass flow rate is around 0.2 kg s^{-1}, whereas the same becomes pronounced as the mass flow rate increases. In conclusion, the compressor with smaller diameter should not be operating under off-design conditions, where the mass flow rate is expected to vary significantly during the operation of the compressor, leading to a degrading efficiency.

Table 2
Parameters for cases 1 and 2

	Inlet tip diameter (m)	Inlet hub diameter (m)	Outlet tip diameter (m)	Outlet hub diameter (m)
Case 1	0.07	0.034	0.15	0.1
Case 2	0.06	0.024	0.14	0.09

Additional studies are performed to investigate the effect of blade inlet setting angle on pressure, efficiency and losses, as shown in Figs. 9a and b and 10, respectively. Both the efficiency and the pressure are lower for smaller setting angles, obviously the losses shown in Fig. 10 has an opposite trend. Given the same mass flow rate under off-design conditions, the efficiency of the compressor gets poorer for the smaller blade inlet setting angle.

5.3. Validation of model

The proposed model was validated against experimental and analytical results from the literature. For experimental comparisons, the parameters for the centrifugal compressor is as shown in Table 3.

Fig. 11 shows the comparison between the VTB simulation results at three different rotational speeds with the experiment

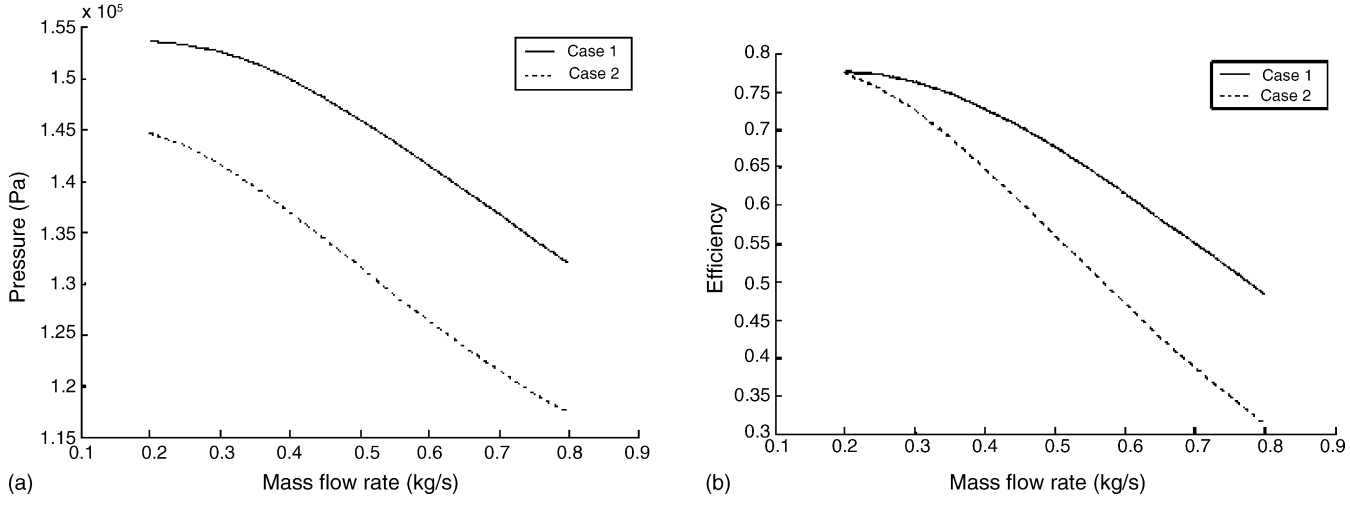

Fig. 8. (a) $\dot{m}$ vs. pressure for different inlet and outlet diameters and (b) $\dot{m}$ vs. efficiency for different inlet and outlet diameters.

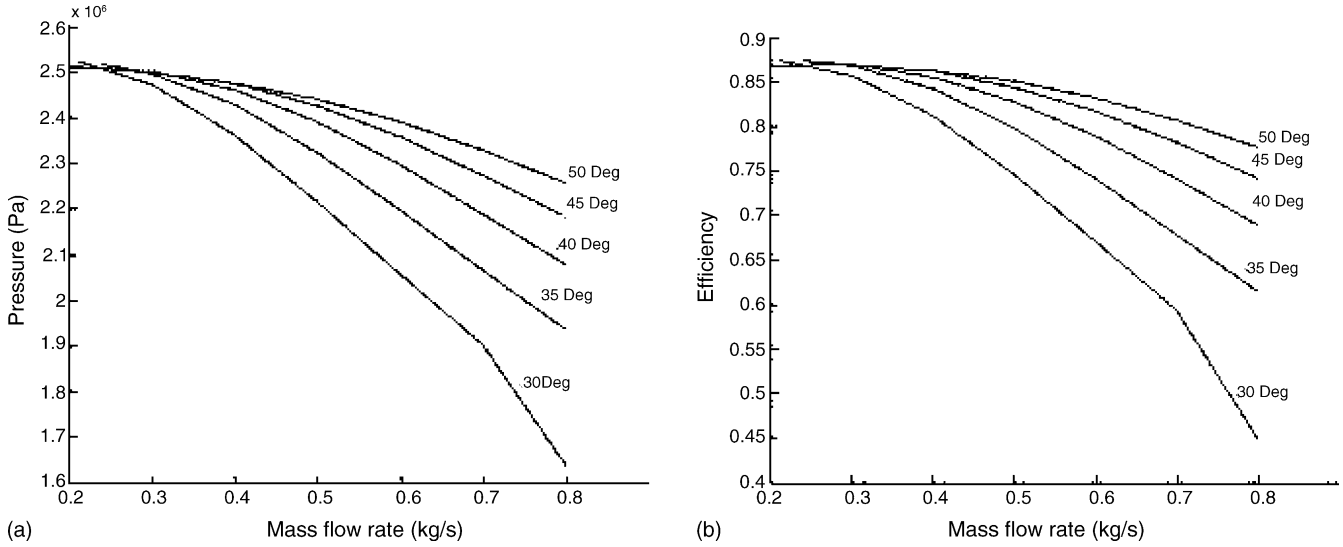

Fig. 9. (a) $\dot{m}$ vs. pressure for various blade inlet setting angle and (b) $\dot{m}$ vs. efficiency for various blade inlet setting angle.

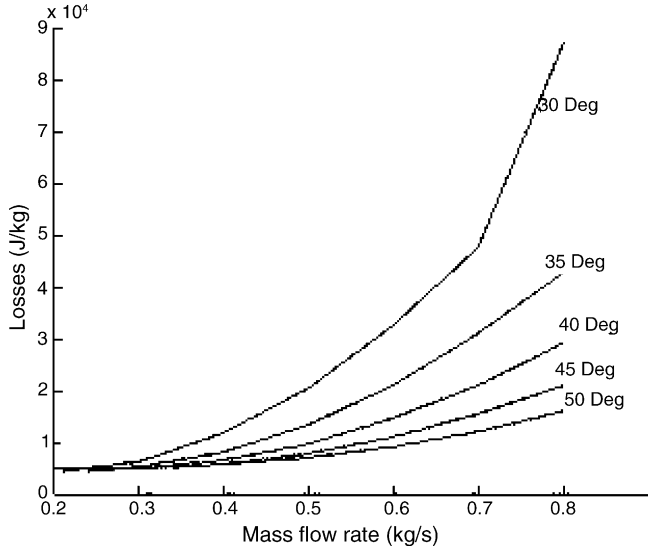

Fig. 10. $\dot{m}$ vs. losses for various blade inlet setting angle.

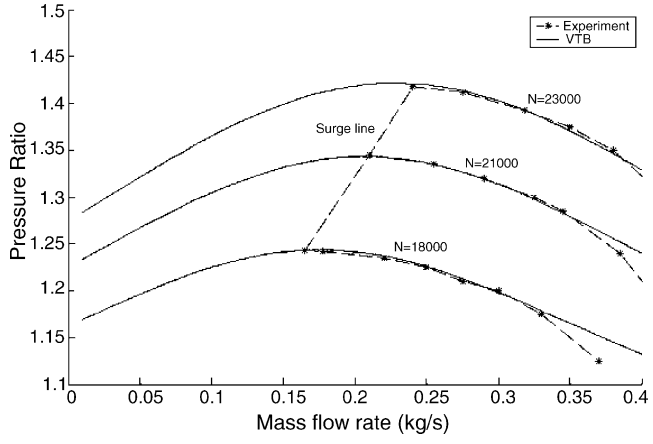

Fig. 11. Comparison between the VTB simulation results and experiment.

results presented in the reference paper [16]. The dimensions used for the model are same as that of the experimental compressor. As shown in the figure, the VTB simulation results match very well with experiment in the neighborhood of the surge line. At the same time, the deviation begins to increase as mass flow rate goes up. The reason for this might be due to some other losses (disc friction, choking, etc.), which are not taken account in our model.

Figs. 12 and 13 show the comparison between the VTB simulation results and the corresponding results presented in the reference paper [1]. The agreement between the results is very good, with VTB slightly over predicting the efficiency and the pressure.

Table 3
Centrifugal compressor parameters used for comparing with the experimental results

Parameter	Value	Parameter	Value
Blade inlet angle (°)	40	Inlet hub diameter (m)	0.054
Vane inlet angle (°)	28	Outlet tip diameter (m)	0.18
Inlet tip diameter (m)	0.106	Outlet hub diameter (m)	0.18

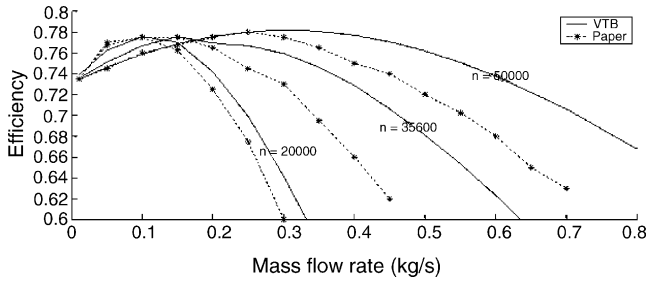

Fig. 12. Comparison between VTB simulation results and paper [1] results in terms of efficiency.

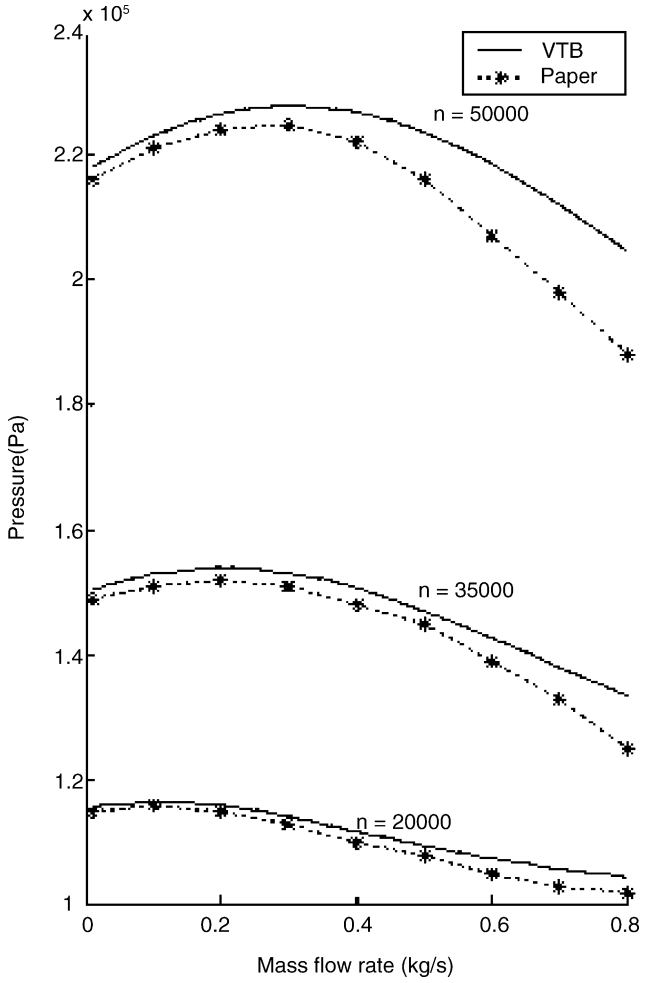

Fig. 13. Comparison between VTB simulation results and paper [1] results in terms of pressure.

5.4. System efficiency

Fig. 14 shows total system efficiency versus mass flow rate and compressor efficiency versus mass flow rate. The effective

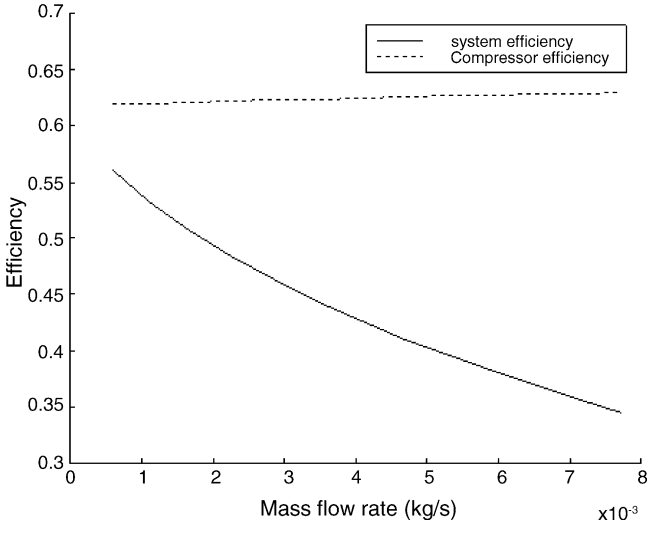

Fig. 14. System efficiency.

Table 4
Parameters for dynamic centrifugal compressor model

Parameter	Value	Parameter	Value
Slip coefficient	0.84	Outlet tip diameter (m)	0.06
Diffuser inlet angle (°)	70	Outlet hub diameter (m)	0.06
Inlet tip diameter (m)	0.0465	Mean impeller channel length (m)	0.025
Inlet hub diameter (m)	0.0158	Mean diffuser channel length (m)	0.006

output of this system is electrical power. The heat power output dissipated into the air is not considered here. The outlet pressure is kept at 120,000 Pa in the simulation. It can be pointed out her that the compressor efficiency remains almost constant because the change in mass flow rate is very small. The simulation parameters for the compressor are shown in Table 4.

6. Conclusion

In this paper, an analytical model for the centrifugal compressor is developed from the first principles where energy transfer is being taken into consideration. The model developed allows the user to predict the compressor performance from the geometric information. In this paper, the incident loss and friction loss are modeled, so are other losses: clearance loss, backward loss and volute loss. A dynamic model for the compressor is then programmed into the VTB simulation environment as a component of an electrical system. From that, we can predict the compressor performance curves such as outlet pressure, efficiency and losses. In addition, surge line obtained from the simulation result can be used to define stable operation range. The dynamic simulation model can be used as a virtual test bed for compressors.

Appendix A

A.1. Velocity triangles for flow through the stage of a centrifugal compressor

Velocity diagrams for flow through the stage of a centrifugal compressor are shown in Fig. A.1.

Fig. A.1a refers to the inlet velocity triangle and (b) to the outlet velocity triangle. All the variables defined in both (a) and (b) will be used for the following energy transfer and losses analysis.

The absolute inlet velocity C_1 is given by

$$C_1 = \frac{1}{\rho_{01} A_1} \dot{m}$$

where ρ_{01} is the constant stagnation inlet density and A_1 is the inlet reference area. The tangential velocity of the impeller U_1 is given by

$$U_1 = \frac{D_1}{2} \cdot \omega = \pi D_1 N$$

where N is the rotational speed of the impeller and D_1 is the average diameter, which is defined as

$$D_1^2 = \frac{1}{2}(D_{t1}^2 + D_{h1}^2)$$

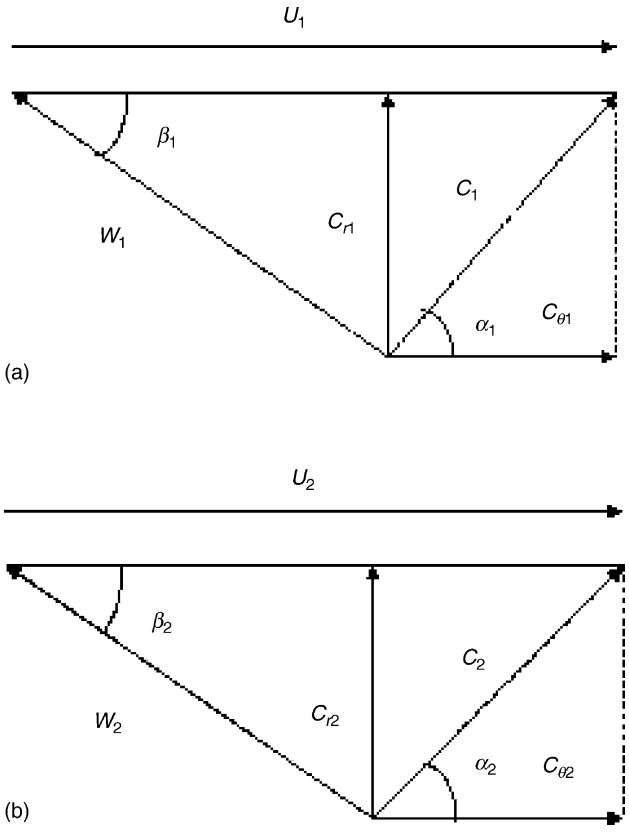

Fig. A.1. (a and b) Velocity triangles for a centrifugal compressor.

where D_{t1} is the inducer tip diameter and D_{h1} is the hub casing diameter.

A.2. *Energy transfer for an ideal compressor*

For the ideal compressor, the ideal specific enthalpy delivered to the fluid will be derived as follows.

The torque equals the change in angular momentum of the fluid in an ideal compressor,

$$\tau_c = \dot{m} \cdot (r_2 C_{\theta 2} - r_1 C_{\theta 1}) \tag{A.1}$$

The power delivered to the fluids is

$$\dot{W}_c = \omega \cdot \tau_c = \omega \cdot \dot{m} \cdot (r_2 C_{\theta 2} - r_1 C_{\theta 1}) = \dot{m} \cdot (U_2 C_{\theta 2} - U_1 C_{\theta 1}) = \dot{m} \cdot \Delta h_{\text{ideal}} \tag{A.2}$$

In order to simplify the analysis, we assumed that there were no stationary pre-whirl vanes and air approaching the impeller did not have a tangential component of velocity.

$$\Delta h_{\text{ideal}} = \frac{\dot{W}_c}{\dot{m}} = C_{\theta 2} \cdot U_2 \tag{A.3}$$

The ratio between $C_{\theta 2}$ and U_2 in a radial vane impeller is called the slip factor, which is defined as

$$\sigma = \frac{C_{\theta 2}}{U_2}$$

From above analysis, the ideal specific enthalpy delivered to the fluid is

$$\Delta h_{\text{ideal}} = \frac{\dot{W}_c}{\dot{m}} = \sigma \cdot U_2^2 \tag{A.4}$$

References

[1] J.T. Gravdahl, O. Egeland, Centrifugal compressor surge and speed control, IEEE Trans. Control Syst. Technol. 7 (September (5)) (1999).
[2] N. Watson, M.S. Janota, Turbocharging the Internal Combustion Engine, MacMillan, New York, 1982.
[3] A. Whitfield, F.J. Wallace, Study of incidence loss models in radial and mixed-flow turbomachinery, in: Proceedings of the Congress of Heat Fluid Flow in Steam and Gas Turbine Plant, University of Warwick, Coventry, UK, April 1973, pp. 122–132.
[4] T.B. Ferguson, The Centrifugal Compressor Stage, Butterworths, London, UK, 1963.
[5] J.D. Denton, Loss mechanisms in turbomachineries, in: Turbomachinery Blade Design Systems, 1999.
[6] B. Lakshimnarayana, Fluid Dynamics and Heat Transfer of Turbomachinery, John Wiley and Sons, Inc., 1995.
[7] D.G. Wilson, The Design of High-Efficiency Turbomachinery and Gas Turbines, The MIT Press, 1984.
[8] K.E. Hansen, P. Jorgensen, P.S. Larsen, Experimental and theoretical study of surge in a small centrifugal compressor, J. Fluids Eng. 103 (1981) 391–394.
[9] F.M. White, Fluid Mechanics, second ed., McGraw-Hill, New York, 1986.
[10] A. Whitfield, F.J. Wallace, Performance prediction for automotive turbocharger compressors, Proc. Inst. Mech. Eng. 189 (12) (1975) 59–67.
[11] C.W. Brice, L.U. Gokdere, R.A. Dougal, The virtual bed: an environment for virtual prototyping, in: Proceedings of International Conference on Electric Ship (ElecShip'98), Istanbul, Turkey, September 1, 1998, pp. 27–31.
[12] G. Cokkinides, B. Beker, VTB Model Developer's Guide, http://vtb.engr.sc.edu/modellibrary/modeldev.asp (online).
[13] G. Cokkinides, B. Beker, RC and AC Models in the VTB Time Domain Solver, The VTB Documentation, December 4, 1998.
[16] J.T. Gravdahl, F. Willems, Modeling for surge control of centrifugal compressors comparison with experiment, in: 39th IEEE Conference on Decision and Control.